Supplement of Atmos. Meas. Tech., 10, 1373–1386, 2017
http://www.atmos-meas-tech.net/10/1373/2017/
doi:10.5194/amt-10-1373-2017-supplement

Atmospheric Measurement Techniques
Open Access

Supplement of

New insights into atmospherically relevant reaction systems using direct analysis in real-time mass spectrometry (DART-MS)

Yue Zhao et al.

Correspondence to: Barbara J. Finlayson-Pitts (bjfinlay@uci.edu)

1. Particle size distributions for amine-reacted diacids and α-cedrene secondary organic aerosol (SOA) particles.

1.1 Amine-reacted diacid particles.

At the exit of the flow reactor, size distributions of the amine-reacted diacid particles were collected using a scanning mobility particle sizer (SMPS, TSI) consisting of an electrostatic classifier (model 3080), a long differential mobility analyzer (DMA, model 3081) and a condensation particle counter (model 3025A or 3776). Typical surface weighted size distributions for (a) malonic acid (C_3), (b) glutaric acid (C_5), and (c) pimelic acid (C_7) reacted particles are presented in Fig. S1, with size distribution statistics given in Table S1. To reflect the ~10% loss of amine-diacid particles in the denuder, a correction factor, C_f, of 1.1 was applied when calculating the fraction of amine in the particles, f_p.

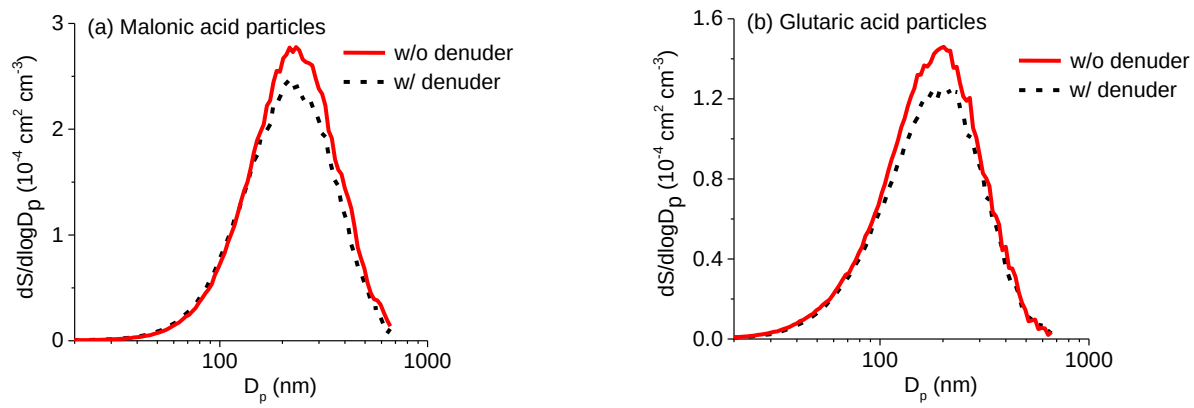

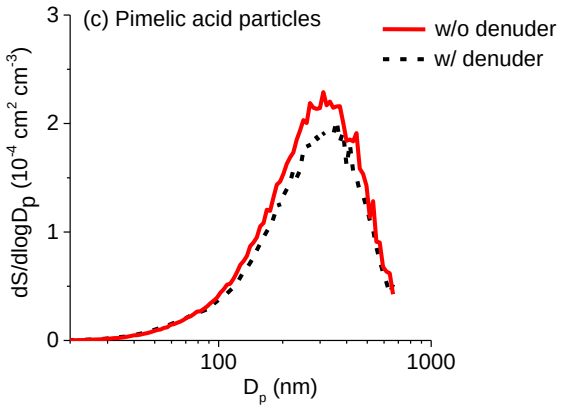

Figure S1. Surface area weighted size distribution of (a) malonic acid, (b) glutaric acid, and (c) pimelic acid particles. The solid and dashed traces correspond to the measurements without or with a denuder, respectively.

Table S1. Size Distribution Statistics for Amine-Reacted Diacid Particles[d]

	Malonic acid (C_3)	Succinic acid (C_4)	Glutaric acid (C_5)	Adipic acid (C_6)	Pimelic acid (C_7)
Surface weighted distribution:					
Total surface area (10^{-4} cm^2 cm^{-3})	1.4 ± 0.3	2.1 ± 0.1	1.1 ± 0.2	1.4 ± 0.2	1.2 ± 0.1
$\overline{D}_{g,S}$ (nm)[a]	239 ± 19	196 ± 8	211 ± 10	209 ± 9	224 ± 8
Volume weighted distribution:					
Total particle volume (10^{-10} cm^3 cm^{-3})	6.8 ± 1.4	8.1 ± 0.8	2.9 ± 0.2	5.0 ± 0.6	5.3 ± 0.5
$\overline{D}_{g,V}$ (nm)[b]	290 ± 22	258 ± 14	269 ± 13	270 ± 9	299 ± 10
Number weighted distribution:					
Total number concentration (10^5 cm^{-3})	1.7 ± 0.5	3.5 ± 0.3	1.7 ± 0.8	2.3 ± 0.2	1.8 ± 0.3
$\overline{D}_{g,N}$ (nm)[c]	103 ± 3	95 ± 2	80 ± 12	81 ± 2	86 ± 4

[a] $\overline{D}_{g,S}$: surface area weighted geometric mean diameter. [b] $\overline{D}_{g,V}$: volume weighted geometric mean diameter. [c] $\overline{D}_{g,N}$: number weighted geometric mean diameter. [d]Error bars represent ±1σ.

1.2 α-Cedrene SOA particles.

Particles exiting the flow reactor at room temperature (T_{PS} = 23°C) were measured by SMPS. A typical size distribution for α-cedrene SOA particles is presented in Fig. S2.

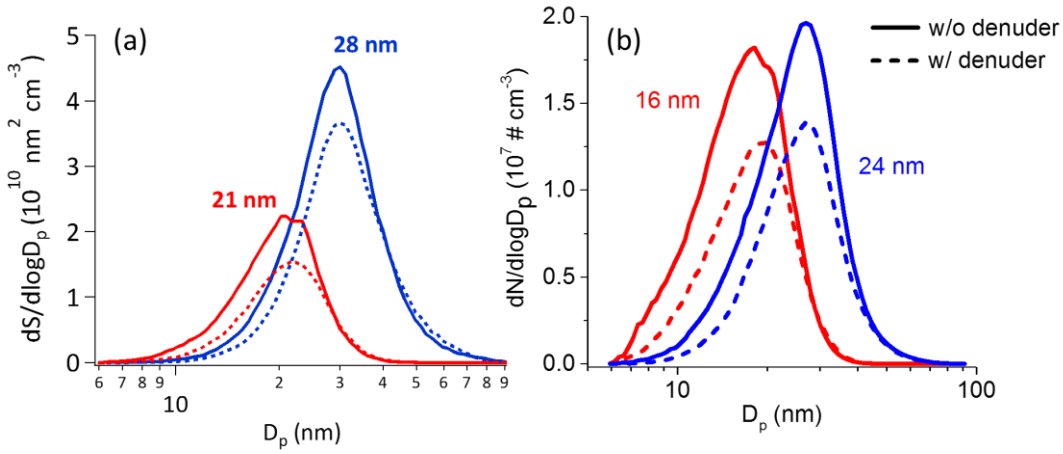

Figure S2. (a) Surface weighted size distribution of α-cedrene SOA with geometric mean diameters ($\bar{D}_{g,S}$) of 21 nm (red) and 28 nm (blue) and (b) number weighted size distribution with geometric mean diameters ($\bar{D}_{g,N}$) of 16 nm (red) and 24 nm (blue) formed in the flow reactor. The solid and dashed traces correspond to the measurements without or with a denuder, respectively at T_{PS} = 23 °C.

2. Temperature in the DART ionization region

The temperature in the ionization region was measured as a function of DART gas temperature both with and without a clean air flow equivalent to that used for the particle stream by placing a thermocouple in the middle of the ionization region. Figure S3 shows that there is no significant difference of the measured temperature in the ionization region regardless of an added flow of air within the region.

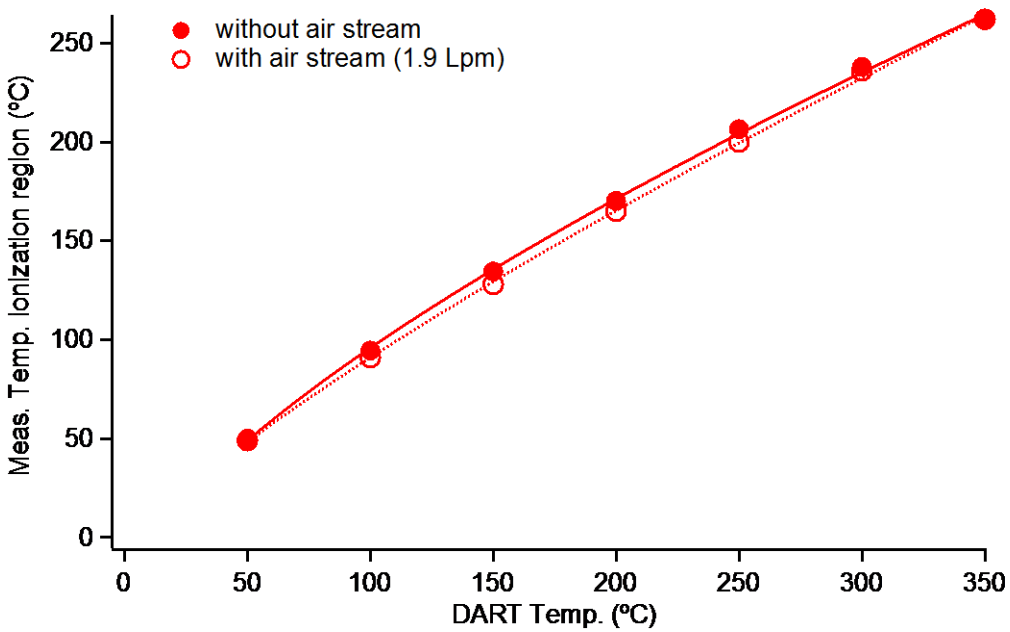

Figure S3. Measured temperature in the ionization region as a function of DART temperature with (open circles) or without (filled circles) added air flow.

3. DART mass spectra of trimethylamine (TMA)-reacted glutaric acid particles and TMA-glutaric acid aqueous standard solution

Amines were observed as their $[M+H]^+$ ions in the positive ion mode (Fig. S4a). Diacids showed fragmentation in the positive ion mode, but only the parent peak was detected in the negative ion mode (Fig. S4b). Both the amine peak in the (+) ion mode and the diacid peak in the (-) ion mode were used for quantification of amines and diacids present in reacted particles exiting the flow reactor. Protonated diacid-amine clusters were not observed either in the mass spectra for particle stream or standard solutions, but the ammonium adduct of the diacid is observed due to the ubiquitous presence of NH_3 in room air. Typical DART mass spectra are shown in Fig. S4 for glutaric acid particles reacted with TMA.

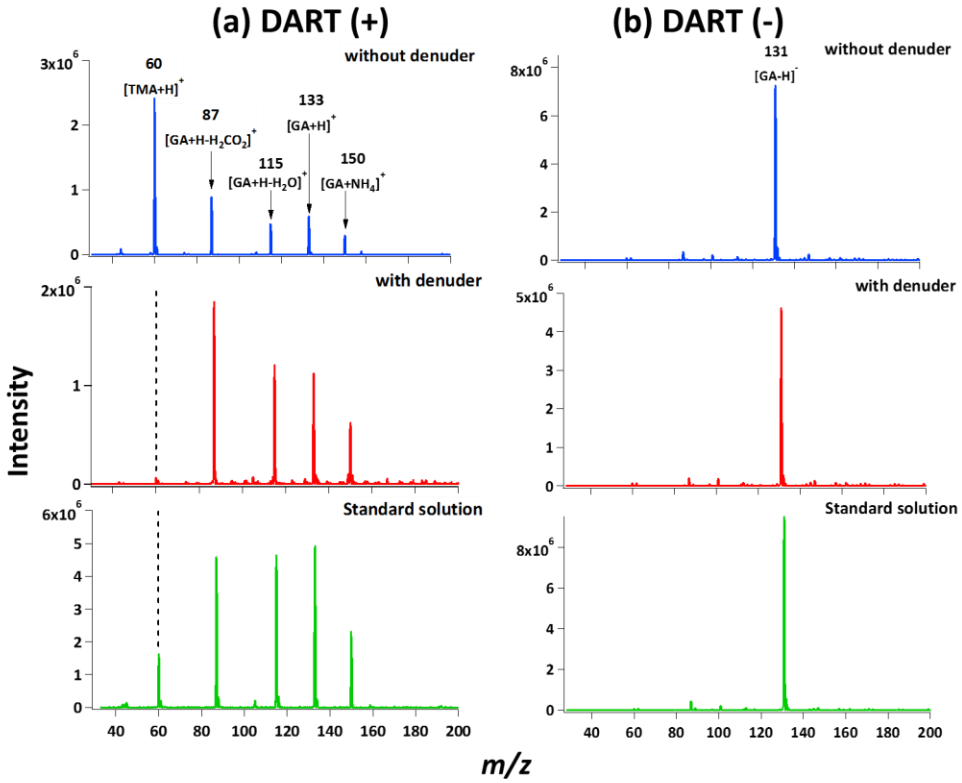

Figure S4. (a) Positive ion mode and (b) negative ion mode DART mass spectra for TMA-reacted glutaric acid (GA) particles from the flow reactor without (blue) or with (red) a denuder, and TMA-glutaric acid aqueous standard solution (green).

4. DART-MS calibrations for the measurement of $R_{B/A}$ values.

Standard solutions of known amine (0.5-10 mM) and diacid (10 mM) concentrations and their corresponding DART-MS intensities were used to determine the $R_{B/A}$ values for amine-reacted diacid particles based on their given intensities measured by DART-MS (see main text). All of the solutions were analyzed in the same manner and five measurements were averaged for each solution.

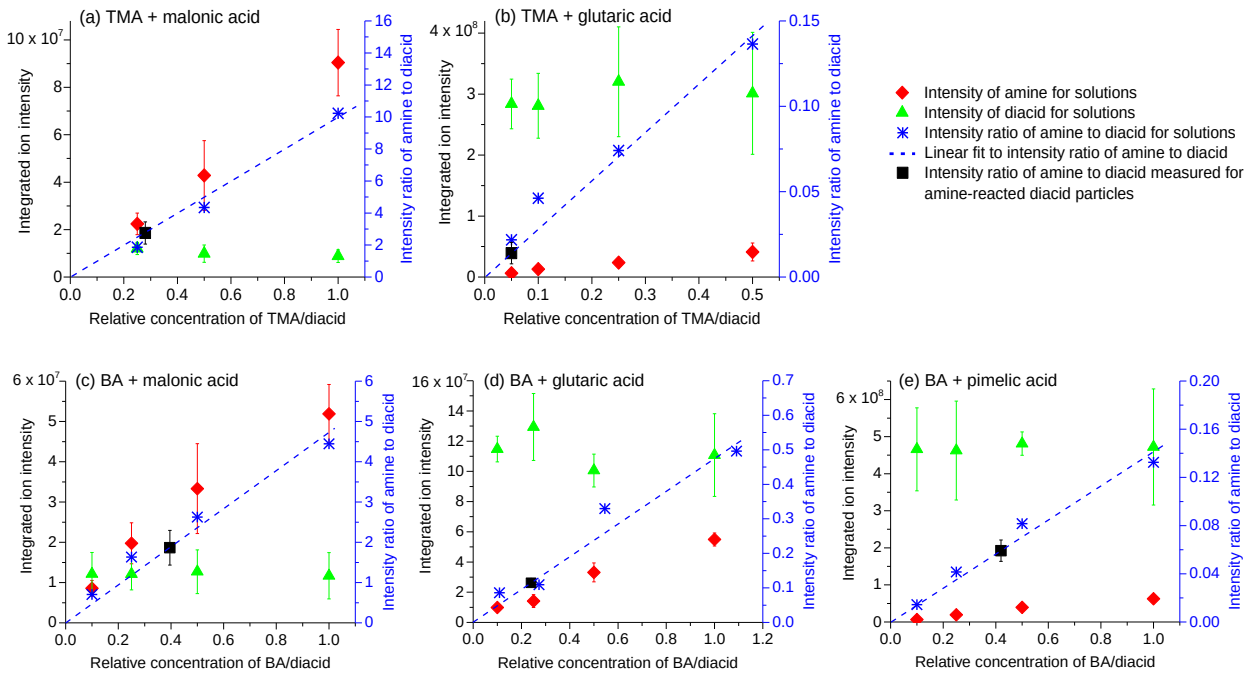

Figure S5. DART-MS signal intensity of amine (red diamond) and diacid (green triangle), as well as their intensity ratios (blue asterisk) as a function of the molar ratio of amine/diacid for different amine-diacid standard solutions. The dashed line is a linear regression fit to the intensity ratios of amine/diacid, i.e. the calibration curve. The black solid squares on each of the calibration curves represent the measured DART-MS intensity ratio of particle-bound amine to diacid, and thus determine the corresponding to the measured molar ratio of amine/diacid ($R_{B/A}$) for amine-reacted diacid particles. Error bars represent ±1σ.

5. HR-ToF-AMS measurements.

5.1 HR-ToF-AMS operating conditions and data analysis.

The chemical composition of TMA-reacted diacid particles from the flow reactor was measured using an Aerodyne high resolution time-of-flight aerosol mass spectrometer (HR-ToF-AMS). In addition, particles of ammonium nitrate and trimethylaminium chloride were sampled by atomizing from aqueous solutions of each salt using a constant output atomizer (TSI, model 3076) and two diffusion dryers (TSI, model 3062) in series. Mass spectra of these salts allowed determination of relative ionization efficiencies (RIE) of NH_4^+ and TMA. All experimental and calibration mass spectra were collected under the same AMS operating conditions: vaporizer temperature = 600 ± 2 °C, ionization energy = 70 eV; filament emission current = 1.2 mA.

5.2 Mass spectra of amine-reacted diacid particles.

Aerosol mass spectra for the amine-reacted malonic acid, glutaric acid, and pimelic acid are shown in Fig. S6. Spectra are normalized to the sum of the total peak intensity and color-coded by the families of ions observed. Fragments of the formula, $C_xH_yN_1^+$, originate from trimethylamine, while $C_xH_yO_z^+$ fragments originate from the diacids. Smaller $C_xH_y^+$ fragments may be generated from both TMA and the diacids (e.g. CH_3^+), but it is clear from Fig. S6 that there are an increasing number of $C_xH_y^+$ fragments as the carbon chain length of the diacid particles increases. The $C_xH_y^+$ fragments account for 9%, 43%, and 56% of total fragments in Fig. S6 for malonic acid, glutaric acid, and pimelic acid diacids, respectively, indicating these fragments are predominantly generated from the diacids.

The relative intensities of $C_xH_yN_1^+$ fragments decrease from malonic acid to pimelic acid indicating that the reactivity of the diacids to TMA decreases with increasing diacid chain length, in agreement with DART-MS data. The ion intensity ratio of amine to diacid present in the particles was calculated from HR-ToF-AMS spectra from the sum of amine peak intensity divided by the sum of diacid intensity for each system, each with RIE = 1. Although the relative intensity of CO_2^+ fragments to the total ion intensity can often be used to identify carboxylic acids (Aiken et al., 2007; Duplissy et al., 2011), quantification of diacids based on CO_2^+ alone for a series of diacids with increasing chain length would lead to large underestimates because of the significant intensity from $C_xH_y^+$. The use of $C_xH_y^+$ fragments to quantify the diacids is

necessary to thoroughly account for all the diacid and allow for comparisons between the systems. A more quantitative assignment of $C_xH_y^+$ fragments to TMA and each diacid is discussed in the next section.

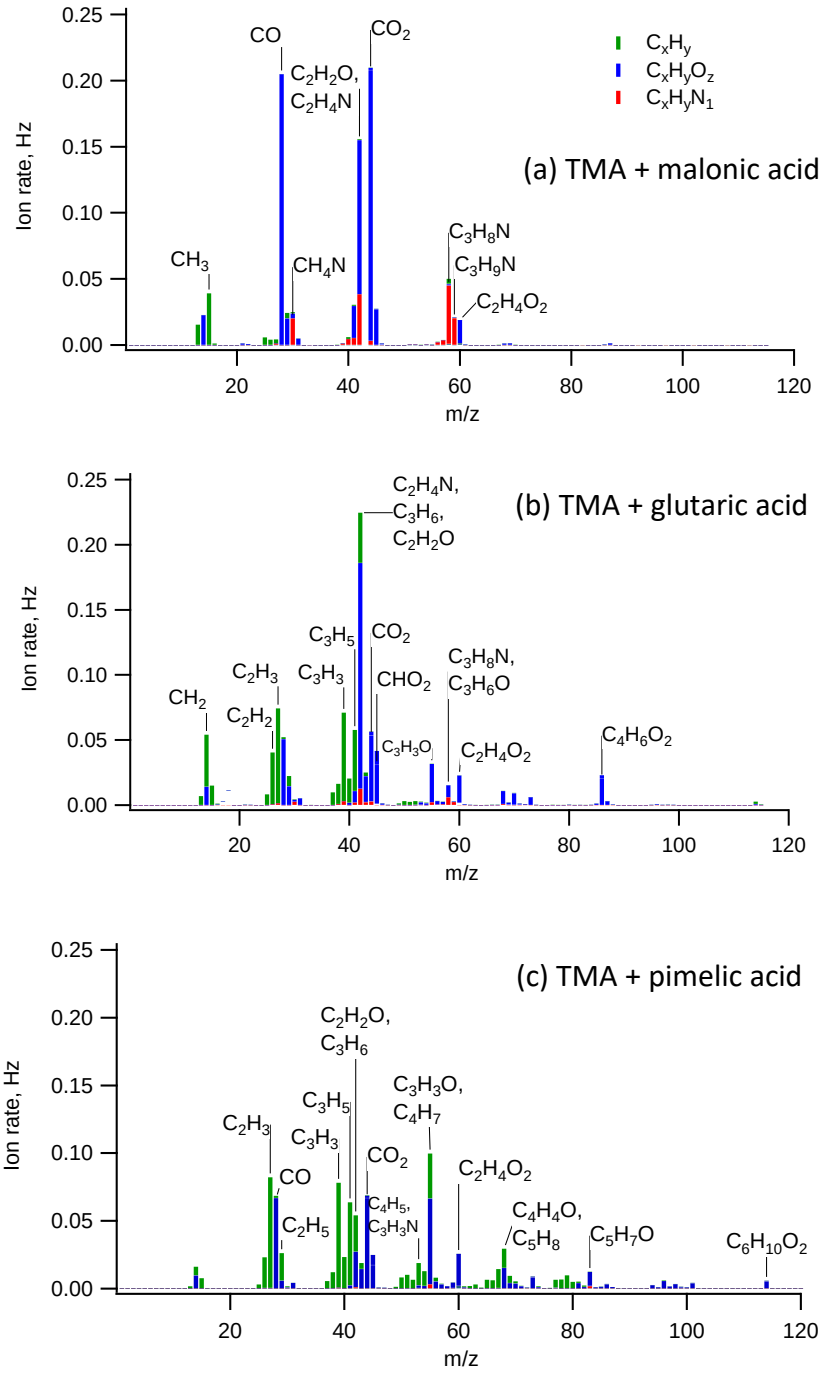

Figure S6. Aerosol mass spectra for TMA-reacted (a) malonic acid (C_3), (b) glutaric acid (C_5), and (c) pimelic acid (C_7) particles. Spectra are normalized to sum to one. Peaks are color-coded

for ion families: $C_xH_y^+$ = green, $C_xH_yO_z^+$ = blue, $C_xH_yN_1^+$ = red, and are stacked to show contributions of ion families to each nominal mass. The labels show some of the fragments that contribute to major peaks.

5.3 Calculation of molar ratios of trimethylamine to diacids.

The mass ratio may be determined from the ion intensity ratio if the RIE of each class of species is known. The accepted RIE for organics (1.4) was used to calculate the mass concentrations of the diacids (Alfarra et al., 2004; Drewnick et al., 2005). On the other hand, TMA, likely existing as an aminium ion, may be expected to have a higher RIE, similar to NH_4^+ (Canagaratna et al., 2007). Previous measurements show a wide range of 5-10 for small amines at similar AMS operating conditions (Silva et al., 2008; McGuire et al., 2014). The RIE of NH_4^+ was determined to be 3.8 ± 0.3 (1σ) through Brute Force Single Particle (BFSP) calibrations using NH_4NO_3 (Fisher, 99.9%) particles of size-selected diameters 300, 350, 400, and 450 nm. To examine the RIE for trimethylaminium ion under our specific operating conditions, particles of trimethylaminium chloride (Sigma-Aldrich, 98%) were sampled by AMS. Equation (S1) shows the relationship between the expected and observed mass intensity ratios.

$$\left(\frac{I_{TMA}}{I_{chloride}}\right)_{expected} = \left(\frac{I_{TMA}}{I_{chloride}}\right)_{observed} \cdot \frac{1/RIE_{TMA}}{1/RIE_{chloride}} \qquad \text{(S1)}$$

The sum of $C_xH_yN_1^+$ fragments and minor $C_xH_y^+$ fragments was used to quantify TMA (I_{TMA}), while the sum of Cl^+ and HCl^+ fragments was used to quantify chloride ($I_{chloride}$). Mass spectra of trimethylaminium chloride are expected to give a mass ratio of amine/chloride of 1.7 (ratio of trimethylaminium (60 g mol^{-1}) to chloride (35.5 g mol^{-1})), but instead gave an observed mass ratio of 4.8. Using the default RIE for chloride (1.3) resulted in an RIE for TMA of 3.7 ± 0.1 (1σ), similar to NH_4^+.

Mass ratios of amine to diacid given by these RIE values (3.7 for TMA, 1.4 for the diacids) are then converted to molar ratios for each TMA-diacid system using the molecular weight (MW) for TMA and each diacid. Equation (S2) shows the parameters used to calculate molar ratios of amine to each diacid, $R_{B/A,AMS}$.

$$R_{B/A,AMS} = \left[\frac{\sum C_xH_yN_1^+}{\sum(C_xH_yO_z^+)+\sum(C_xH_y^+)} \cdot \frac{1/RIE_{amine}}{1/RIE_{acid}}\right] \cdot \frac{MW_{acid}}{MW_{amine}} \quad \text{(S2)}$$

The sum of $C_xH_y^+$ ions was included in the quantification of the diacid because these ions exhibit increasing ion intensity for each diacid as the carbon number of the diacid increases. However, a small contribution of $C_xH_y^+$ ions from TMA was also observed from TMA in trimethylaminium chloride mass spectra. In order to account for the contribution of $C_xH_y^+$ from TMA in trimethylaminium chloride particles, the ratios of major $C_xH_y^+$ ions to the intensity of the $C_3H_8N^+$ peak (largest amine peak) were determined from mass spectra of trimethylaminium chloride spectra. These ratios are expected to be similar in TMA-reacted diacid particle experiments. By far, the major $C_xH_y^+$ ion observed in trimethylaminium chloride spectra was CH_3^+, with a relative intensity of 0.58 to $C_3H_8N^+$. Smaller $C_xH_y^+$ peaks observed from TMA were $C_2H_3^+$ (*m/z* 27) and $C_2H_5^+$ (*m/z* 29) with relative intensities to $C_3H_8N^+$ of 0.10 and 0.11, respectively. These peaks are resolved from other ions at the same nominal mass. In TMA-reacted diacid particle mass spectra, any intensity of these $C_xH_y^+$ ions that was in excess of these ratios was attributed to the diacid.

Figure S7 shows the molar ratios determined for reaction of TMA with diacid particles with and without the correction presented above, as well as without adding any contribution from $C_xH_y^+$ for both TMA and each diacid. The correction for $C_xH_y^+$ from TMA is fairly minor, resulting in a 7% increase in the molar ratio calculated for TMA+malonic acid, 1% for TMA+glutaric acid, and 0.3% for TMA+pimelic acid. It is clear that larger $C_xH_y^+$ fragments begin to contribute significantly to the mass spectrum for glutaric acid particles and pimelic acid particles (decreasing the ratio by a factor of two for the latter). The molar ratios reported in Table 1 of the main text are those including $C_xH_y^+$ fragments with the correction discussed for TMA.

Collection efficiencies of amine-reacted diacid particles in the HR-ToF-AMS may be larger than those of the pure diacid particles, but were assumed to be equal here. Amine reactions with monocarboxylic acids in which the acid is fully titrated have been reported to create liquid particles (Lavi et al., 2015). If this is also true for amine-reacted diacid particles, it would decrease particle bounce on the HR-ToF-AMS vaporizer and increase collection efficiency relative to diacid particles that remain unreacted or less reacted. In this case, $R_{B/A}$ could be overestimated.

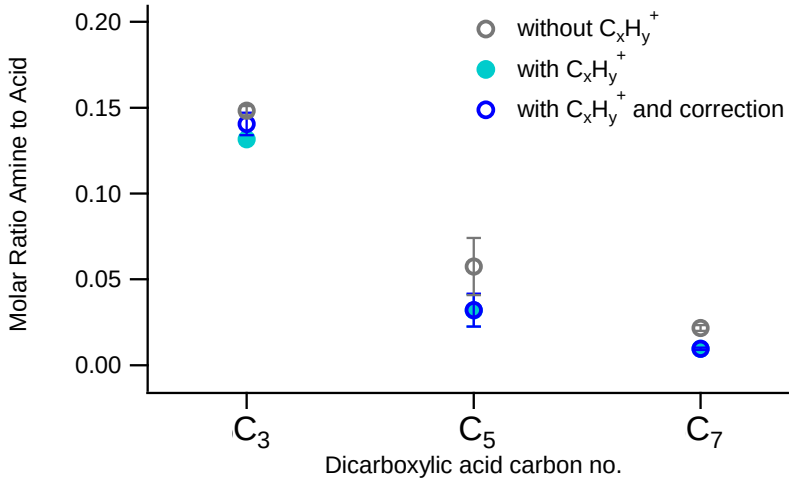

Figure S7. Molar ratio of amine to diacid observed for TMA-reacted malonic (C_3), glutaric (C_5), and pimelic (C_7) acid particles. Mass ratios (not shown) were determined by AMS using an RIE of 3.7 ± 0.1 (1σ) for TMA and the default RIE for all organics of 1.4 for each diacid and converted to molar ratios using Eq. (S2). Error bars represent 1σ of either the standard deviation of replicate measurements or the propagation of mass spectral errors and the amine RIE measurement uncertainty, whichever is greatest.

6. Estimation of the probe depth for pimelic acid particles based on their saturation vapor pressures

Chan et al. (Chan et al., 2013) used DART-MS to measure the probe depth of succinic acid (C_4), adipic acid (C_6), and suberic acid (C_8). They found that the measured probe depth is correlated with the vapor pressure (Bilde et al., 2015) of the diacids, with a measured probe depth of ~10 nm for succinic acid ($P_{sat} = 7.7 \times 10^{-10}$ atm), ~4.5 nm for adipic acid ($P_{sat} = 1.9 \times 10^{-10}$ atm), and ~1 nm for suberic acid ($P_{sat} = 3.3 \times 10^{-11}$ atm). Using the linear regression from this relationship (Fig. S8) and the vapor pressures of malonic acid, glutaric acid, and pimelic acid, respectively, probe depths for these acids were estimated. Although some uncertainty remains in the determination of the absolute probe depth using this approach, this method allows to estimate the relative probe depth between the odd acids tested in the present study. This extrapolation yields a probe depth for glutaric acid (and malonic acid) which is a factor of 8 larger than that of pimelic acid allowing for a corrected $R_{B/A}$ value of 0.05 for butylamine reacted pimelic acid particles.

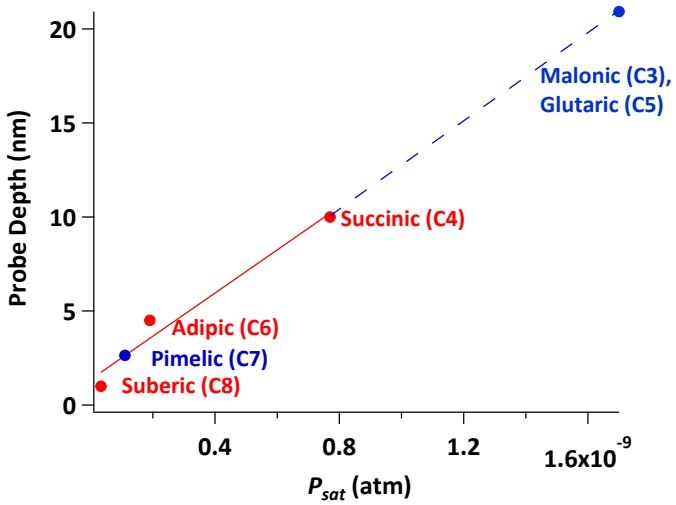

Figure S8. Linear relationship of the probe depth as a function of saturation vapor pressure (P_{sat}) for even-diacids as reported by Chan et al. (Chan et al., 2013) The red trace represents the linear regression for the even diacids: probe depth (nm) = (1.2×10^{10} nm/atm * P_{sat}) + 1.4.

7. Number of TMA molecules ($N_{p\text{-}amine}$) present in TMA-reacted diacid particles

Table S2. $N_{p\text{-}amine}$ values for TMA-reacted diacid systems based on DART-MS measurements.

	C_3	C_4	C_5	C_6	C_7
$N_{p\text{-}amine}$ (10^{11} molecule cm^{-3})	3.8 ± 1.1	ND	0.42 ± 0.02	ND	ND

ND: not detected. Error bars are ±1σ.

8. Evaluation of potential artifacts in DART-MS.

The ionization reactions in the DART ion source can generate reactive oxygen species such as OH and HO_2 radicals, and superoxide anion (O_2^-), along with different reagent ions (Cody et al., 2005; Gross, 2014). These species may lead to in-source oxidation of organic species, in particular for unsaturated compounds. In addition, there may be gas phase ion clustering of organic compounds in the DART ion source, which can lead to the formation of high molecular weight (HMW) species, which has been shown to occur with some ionization techniques such as ESI-MS (Gao et al., 2010; Muller et al., 2009) and CIMS with protonated water clusters or acetate as reagent ions (Aljawhary et al., 2013). In this work, these possible ionization artifacts in the DART source are evaluated to validate the interpretation of DART-MS data. Different standards including α-cedrene, C_3-C_7 diacids, hexadecanedioic acid (Sigma-Aldrich, 96%), pinonic acid (Sigma-Aldrich, 98%), and oleic acid (Sigma-Aldrich, ≥ 99%) were analyzed in the negative ion mode under DART source conditions identical to those for online particle measurements. α-Cedrene was analyzed by directly introducing its gas stream (138 ppb) into the DART ionization region. Other standards were analyzed individually by dipping a clean melting point capillary tube into their pure compounds or aqueous solutions (10 mM) and then placing it directly into the DART ionization region. In addition, the α-cedrene SOA stream, which was heated to 50 ^{o}C before entering into the DART ionization region, was analyzed in some experiments at a lower DART gas temperature (100 or 200 ^{o}C) than the temperature (350 ^{o}C) used for routine measurements. At these low temperatures, very low volatility HMW products in the SOA would not be effectively vaporized and the HMW ions observed in the mass spectrum,

if any, should be mainly formed by the in-source ion clustering of relatively high volatility products desorbed from SOA particles.

Figure S9a shows the DART(-) (negative ion mode) mass spectrum of 138 ppb gas phase α-cedrene. No ion signal due to α-cedrene itself corresponding to its $[M – H]^-$ (*m/z* 203) or $[M]^-$ (*m/z* 204) parent ion is observed in the mass spectra, consistent with previous studies which showed that alkenes can only be detected in the positive ion mode (Nah et al., 2013). However, strong peaks at *m/z* 235 and *m/z* 251 and relatively smaller peaks at *m/z* 237 and *m/z* 253, which are the oxidation products of α-cedrene as discussed later, are observed in the mass spectra, suggesting that oxidation of α-cedrene occurs in the DART source. Analysis of an oleic acid standard using DART-MS also showed multiple peaks corresponding to its oxidation products such as azelaic acid (from oxidative cleavage of the double bond) consistent with the detection by other techniques (Zahardis and Petrucci, 2007), OAO (one oxygen atom added to oleic acid), and OAO_2 (two oxygen atoms added) (Chan et al., 2013) with intensities of ~ 5-10% of the oleic acid parent peak. In contrast, no obvious peaks indicating oxidation chemistry were observed in DART(-) mass spectra for other standards that do not have a C=C bond. For DART-MS analysis of α-cedrene SOA particles, the particle stream was first passed through a denuder to remove the gas phase species including the unreacted α-cedrene. Additionally, since α-cedrene contains only one C=C bond, the oxidation products are unlikely to have C=C bonds. Therefore, it is expected that the DART-MS analysis presented below would not suffer from an in-source oxidation artifact.

Figures S9b and S9c show the DART(-) mass spectra of α-cedrene SOA particles where the particle stream was heated to T_{PS} = 50 ^oC and the DART gas temperature (T_{DART}) was either 100 or 200 ^oC. Only low molecular weight (LMW) ions are observed in the mass spectra, as expected if the HMW products in the SOA particles were not effectively vaporized under these analysis conditions. The absence of HMW ions in the mass spectra also suggests that the in-source clustering of components of α-cedrene SOA particles is not important. The DART(-) mass spectra of standard compounds also show negligible contributions from HMW ions except for malonic acid, for which the acid dimer is observed with its intensity being ~ 20% of that of the monomer.

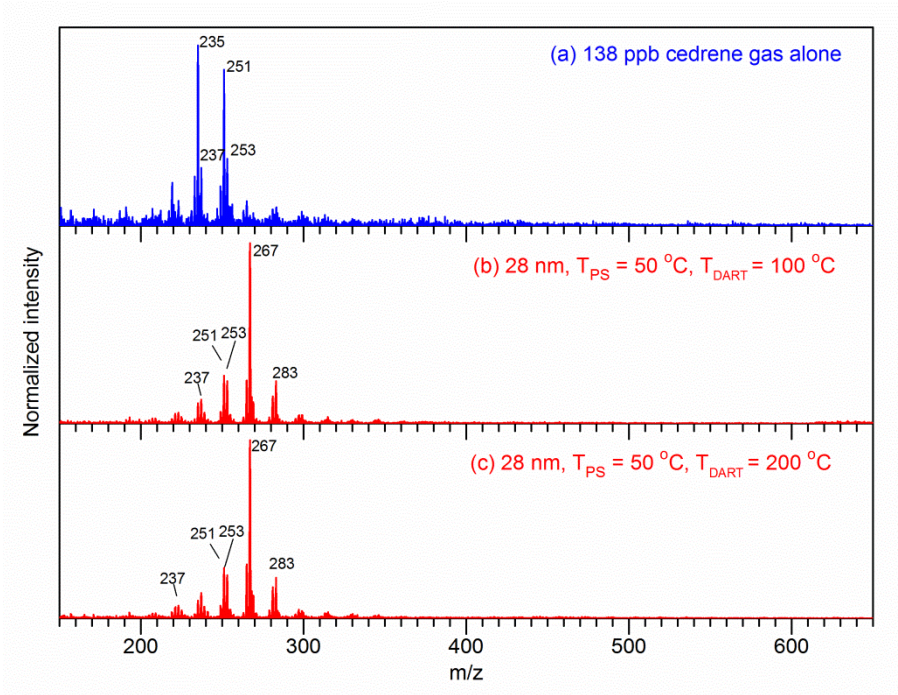

Figure S9. DART(-) mass spectra of (a) α-cedrene gas, (b) α-cedrene SOA particles at T_{DART} = 100 ºC, and (c) α-cedrene SOA particles at T_{DART} = 200 ºC. T_{PS} denotes the particle stream heating temperature before introduction into the ionization region, which is 50 °C for (b) and (c). T_{DART} represents the DART gas temperature.

References:

Aiken, A. C., DeCarlo, P. F., and Jimenez, J. L.: Elemental analysis of organic species with electron ionization high-resolution mass spectrometry, Anal. Chem., 79, 8350-8358, 2007.

Alfarra, M. R., Coe, H., Allan, J. D., Bower, K. N., Boudries, H., Canagaratna, M. R., Jimenez, J. L., Jayne, J. T., Garforth, A. A., and Li, S.-M.: Characterization of urban and rural organic particulate in the Lower Fraser Valley using two Aerodyne aerosol mass spectrometers, Atmos. Environ., 38, 5745-5758, 2004.

Aljawhary, D., Lee, A. K. Y., and Abbatt, J. P. D.: High-resolution chemical ionization mass spectrometry (ToF-CIMS): application to study SOA composition and processing, Atmos. Meas. Tech., 6, 3211-3224, 2013.

Bilde, M., Barsanti, K., Booth, M., Cappa, C. D., Donahue, N. M., Emanuelsson, E. U., McFiggans, G., Krieger, U. K., Marcolli, C., Tropping, D., Ziemann, P., Barley, M., Clegg, S., Dennis-Smither, B., Hallquist, M., Hallquist, A. M., Khlystov, A., Kulmala, M., Mogensen, D., Percival, C. J., Pope, F., Reid, J. P., da Silva, M. A. V. R., Rosenoern, T., Salo, K., Soonsin, V. P., Yli-Juuti, T., Prisle, N. L., Pagels, J., Rarey, J., Zardini, A. A., and Riipinen, I.: Saturation vapor pressures and transition enthalpies of low-volatility organic molecules of atmospheric relevance: from dicarboxylic acids to complex mixtures, Chem. Rev., 115, 4115-4156, 2015.

Canagaratna, M., Jayne, J., Jimenez, J., Allan, J., Alfarra, M., Zhang, Q., Onasch, T., Drewnick, F., Coe, H., and Middlebrook, A.: Chemical and microphysical characterization of ambient aerosols with the Aerodyne aerosol mass spectrometer, Mass Spectrom. Rev., 26, 185-222, 2007.

Chan, M. N., Nah, T., and Wilson, K. R.: Real time *in situ* chemical characterization of sub-micron organic aerosols using direct analysis in real time mass spectrometry (DART-MS): the effect of aerosol size and volatility, Analyst, 138, 3749-3757, 2013.

Cody, R. B., Laramee, J. A., and Durst, H. D.: Versatile new ion source for the analysis of materials in open air under ambient conditions, Anal. Chem., 77, 2297-2302, 2005.

Drewnick, F., Hings, S. S., DeCarlo, P., Jayne, J. T., Gonin, M., Fuhrer, K., Weimer, S., Jimenez, J. L., Demerjian, K. L., and Borrmann, S.: A new time-of-flight aerosol mass spectrometer (TOF-AMS)—instrument description and first field deployment, Aerosol Sci. Tech., 39, 637-658, 2005.

Duplissy, J., DeCarlo, P. F., Dommen, J., Alfarra, M. R., Metzger, A., Barmpadimos, I., Prevot, A. S., Weingartner, E., Tritscher, T., and Gysel, M.: Relating hygroscopicity and composition of organic aerosol particulate matter, Atmos. Chem. Phys., 11, 1155-1165, 2011.

Gao, Y. Q., Hall, W. A., and Johnston, M. V.: Molecular composition of monoterpene secondary organic aerosol at low mass loading, Environ. Sci. Technol., 44, 7897-7902, 2010.

Gross, J. H.: Direct analysis in real time-a critical review on DART-MS, Anal. Bioanal. Chem., 406, 63-80, 2014.

Lavi, A., Segre, E., Gomez-Hernandez, M., Zhang, R. Y., and Rudich, Y.: Volatility of atmospherically relevant alkylaminium carboxylate salts, J. Phys. Chem. A, 119, 4336-4346, 2015.

McGuire, M. L., Chang, R. Y. W., Slowik, J. G., Jeong, C. H., Healy, R. M., Lu, G., Mihele, C., Abbatt, J. P. D., Brook, J. R., and Evans, G. J.: Enhancing non-refractory aerosol

apportionment from an urban industrial site through receptor modeling of complete high time-resolution aerosol mass spectra, Atmos. Chem. Phys., 14, 8017-8042, 2014.

Muller, L., Reinnig, M. C., Hayen, H., and Hoffmann, T.: Characterization of oligomeric compounds in secondary organic aerosol using liquid chromatography coupled to electrospray ionization Fourier transform ion cyclotron resonance mass spectrometry, Rapid Commun. Mass Spectrom., 23, 971-979, 2009.

Nah, T., Chan, M., Leone, S. R., and Wilson, K. R.: Real time *in situ* chemical characterization of submicrometer organic particles using direct analysis in real time-mass spectrometry, Anal. Chem., 85, 2087-2095, 2013.

Silva, P. J., Erupe, M. E., Price, D., Elias, J., GJ Malloy, Q., Li, Q., Warren, B., and Cocker III, D. R.: Trimethylamine as precursor to secondary organic aerosol formation via nitrate radical reaction in the atmosphere, Environ. Sci. Technol., 42, 4689-4696, 2008.

Zahardis, J., and Petrucci, G. A.: The oleic acid-ozone heterogeneous reaction system: products, kinetics, secondary chemistry, and atmospheric implications of a model system - a review, Atmos. Chem. Phys., 7, 1237-1274, 2007.